Reorganization of Nanopatterned Polymer Brushes by the AFM Measurement Process

Michael Patra and Per Linse*

Physical Chemistry 1, Center for Chemistry and Chemical Engineering, Lund University, P.O. Box 124, SE-221 00 Lund, Sweden

Received March 22, 2006; Revised Manuscript Received April 10, 2006

ABSTRACT: The interaction between a nanopatterned polymer brush and a rigid pyramidal body representing an AFM tip has been investigated using molecular dynamics (MD) simulation. The computed forces for varying position and penetration depth are systematically contrasted with the density and pressure tensor profiles of the unperturbed brush. For weak penetration of the AFM tip in the brush, we find that the force can quantitatively be computed from the properties of the unperturbed brush after folding with the geometry of the AFM tip. This steric effect leads to a force profile that is significantly wider than the physical brush. The structure of the perturbed brush has also been examined, and we show that for deep penetration of the AFM tip more than half of the force originates from the reorganization of the brush.

I. Introduction

After recent advances in the nanostructuring of surfaces, polymers can now be end-grafted on structures that are on the nanometer scale in one or both of their dimensions.[1,2] The recent progress in the production of patterned polymer structures has unfortunately only partially been matched by advances in the experimental methods to measure the properties of such systems.[3] Available contactless methods, for example, optical methods, averaging the brush properties over areas that are larger than the nanopattern such that all spatial resolution is lost.

To retain sufficient spatial resolution, atomic-force microscopy (AFM) is conventionally used.[4−7] The necessary contact between the AFM tip and the polymer brush — this contact is permanent in contact mode and temporary in tapping mode measurements — distorts the brush and thus the object that it intends to study.[8] Also the details of the shape of the AFM tip are important for the interpretation of the measurement results.[9] The relation between the shape of the polymer brush and the results of AFM measurements thus is nontrivial.[10,11] A direct interpretation of experimental AFM results without accounting for the response of the brush on the external force seems to contradict previous numerical results of the brush shape.[12]

The interaction between an AFM tip and a patterned polymer brush bears resemblance to other problems that have received growing interest lately, for example, to studies of the interaction between an object and a homogeneously grafted polymer brush[13,14] and to the heterogeneity appearing in polymer glasses.[15,16]

AFM measurements of nanopatterned polymer brushes are a prime example of a more general and fundamental class of problems, namely the response of soft matter to external forces. Previous work in this context is limited and focuses mainly on the interaction between two polymer-covered surfaces.

Earliest work on the interaction between a single homogeneously grafted polymer brush and an external object neglected the effect of splay[17−19] and hence the essence of the problem. The use of an infinitely large plane as the external object[20] neglects splay as well. Other studies only are applicable to very small objects.[21,22] A step toward an understanding of the role of the splay was done by simulations of the interaction between a sphere and a homogeneously grafted polymer brush.[14] A nanopatterned polymer brush, however, is a much more complicated system as its correlation length is of the same order as the size of the system. Therefore, the brush can evade to the side, which is impossible for the homogeneously grafted brush, making the nanopatterned brush effectively "softer".

The force measured in an AFM experiment is rarely the quantity that one is ultimately interested in. The noteworthy exception to this statement are studies of the chemical nature of the brush surface where the sticking force between the AFM tip and the brush directly supplies the sought-after information.[5] In most other cases, the measured force F first has to be converted, or "gauched", to yield, for example, the brush density ρ. However, already for a homogeneously grafted brush, computing the density ρ is not possible from the knowledge of the force F alone — instead, additional information about the brush is needed,[14] such as its grafting density, and this information frequently might not be available.

Still, for the case of a homogeneously grafted polymer brush, a relation between F and ρ always exists and does not depend on the transversal position of the AFM tip, and the same is true also for all other quantities. All of this changes when a patterned polymer brush is considered instead. Even for the same brush, identical values of the force F now correspond to different values of the density ρ (or some other quantity of interest). This prevents a deeper understanding of the grafted brush's properties from a direct interpretation of AFM results.

Thus, the need to understand the response of nanopatterned polymer brushes to local external forces is both fundamental and practical. In this contribution, we will report on such a study of a polymer brush that is representative for a wider range of systems. We have performed molecular-dynamics (MD) simulations of the interaction between a patterned polymer brush and an AFM tip. The force onto the AFM tip is computed from the interaction between the polymer segments and the particles representing the AFM tip. This directly simulated force profile is complemented by force estimates using the pressure tensor profile of the polymer brush in the absence of an AFM tip.

II. Setup

We restrict ourselves to the experimentally most common setup. Consider a surface in the $z = 0$ plane. Polymers are end-attached

10.1021/ma0606410 CCC: $33.50
Published on Web 05/17/2006

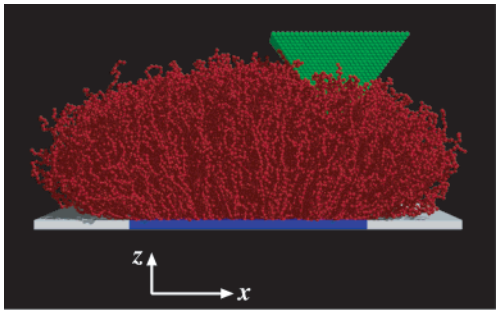

Figure 1. Snapshot illustrating a pyramid representing the AFM tip (green) penetrating into a nanopatterned polymer brush (red). The polymer chains are grafted onto the blue region. The orientation of the coordinate system is also indicated.

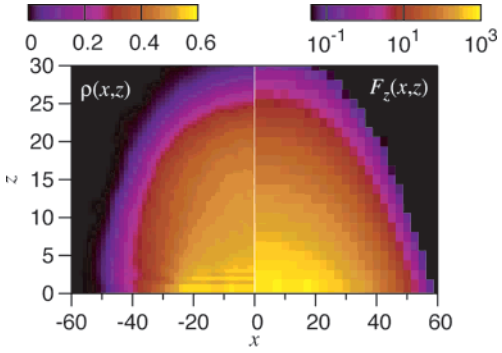

Figure 2. Density of an unperturbed brush $\rho(x, z)$ and vertical force $F_z(x, z)$ onto the AFM tip. The width of the grafted region is $\Delta = 50$ and it extends from $x = -25$ to 25. Please note the different scales of the horizontal and vertical axis in this and all other related figures.

with the grafting density σ (number of chains per unit area) onto an infinitely long stripe of width Δ running in the y-direction. The polymers are described as freely jointed chains composed of N particles connected by harmonic bonds. The AFM tip is modeled as a pyramid build from the same particles as the polymers, see Figure 1. The slope of the tip, x:z, is $1{:}\sqrt{2}$, and the planar sides of the pyramids thus are tilted by 35° against the vertical direction. The apex of the pyramid is effectively slightly rounded as the single particle at the apex had been removed. The height of the pyramid was sufficient to ensure that the pyramid fully extends to the outside of the brush. It should be stressed that, while an unperturbed brush in this geometry is a two-dimensional problem, the AFM tip is three-dimensional, and the properties of the perturbed brush thus depend on all three coordinates.

In this study, we focus on the values $N = 50$, $\Delta = 50$, and $\sigma = (1/3)^2$. For $\Delta \ll N$, no well-defined brush is formed, and for $\Delta \gg N$, the nanoproperty of the brush is lost,[12] such that $N \approx \Delta$ is a good choice for the purpose of our study. (All lengths are measured in units of the bond length.) This is complemented by two additional setups where Δ respectively σ are reduced by 60%. Further aspects on the model and methods used are provided in the Appendix.

Additional simulations of the polymer brush without the AFM tip were made to determine number density $\rho(x, z)$ and pressure tensor $\vec{p}(x, z)$ profiles of an unperturbed brush.

III. Results

A. Brush Density and Vertical Force. The density $\rho(x, z)$ of the unperturbed polymer brush is displayed in Figure 2 (left). For symmetry reasons, only half of the brush is shown. The density is identical to earlier results[12] up to some small differences caused by different modeling of bonded and nonbonded potentials. For our choice $\Delta = N$, the polymers in the center ($x = 0$) are stretched — the traditional definition of a brush thus is fulfilled — while at the same time there is a considerable overshot of the brush over the grafting region. The latter is quantified by the excess brush width w,[12] and, as w and brush width h are approximately equal, the polymers are comparably stretched everywhere only their average orientation differs.

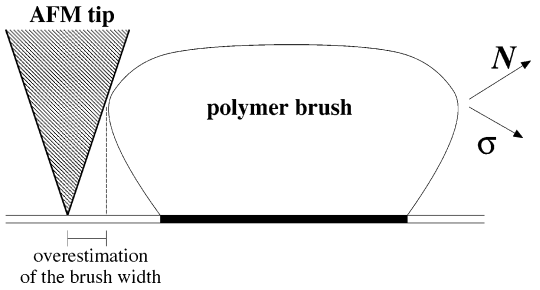

Figure 3. Sketch of the steric effect of the finite slope of the AFM tip. The arrows on the right indicate how the contact point moves if N respectively σ are increased.

Figure 2 (right) shows the vertical force $F_z(x, z)$ onto the AFM tip. The vertical force component is the one that one intends to measure in a typical AFM setup. The spatial variation of F_z resembles that of the brush density, but significant differences are present. The region with nonvanishing F_z is larger than the region with nonvanishing ρ. This effect is especially pronounced near the stripe edge. It is a steric effect that is due to the finite slope of the AFM tip. We will study this quantitatively in section III.C, but the qualitative effect is easily explained already by the simple sketch in Figure 3.

Whenever any part of the AFM tip touches the polymer brush, a force acts on the tip — even when the apex of the AFM tip is not in contact with the brush. As the sketch shows, this leads to an overestimation of the brush width. Quantitatively, this depends on the slope of the AFM tip as well as on the height above the grafting surface of the contact point between the tip and the brush. This contact point is defined by the condition that the slope at this point is equal to the AFM tip angle α, but due to the large curvature of the brush one can in practice take the point of largest overshot instead. An increase in either N or σ shifts this point outward, but the vertical motion is opposite. In particular, for small σ (as in most experimental situations) this point occurs at large height, and the overestimation of the brush width is large.

Of course, a "real" polymer brush does not have a well-defined surface, and the force onto the AFM tip is not simply either "on" or "off". In section III.C, we will thus present a more quantitative analysis. However, already our qualitative analysis shows that the brush width will be overestimated by an amount $N \tan\alpha$ with a prefactor smaller than but of order unity.

B. Effective Brush Density. A direct comparison between forces and densities is problematic as these two quantities carry different units. It is therefore instructive to "recalibrate" the forces on the AFM tip in terms of densities, as already mentioned in the Introduction. One possibility for such a recalibration would be to use the force-density relation for a homogeneously grafted polymer. We decided to use our simulation data for the center of the nanopatterned brush, $x = 0$, as provided in Figure 2, for this mapping. The obtained relation is given in Figure 4.

Figure 5 (left) provides the density of the unperturbed polymer brush $\rho(x, z)$ while Figure 5 (right) shows the effective brush density $\rho_{\text{eff}}(x, z)$. The latter one is the result of applying the $\rho(F_z)$-mapping onto the vertical force $F_z(x, z)$. We denote this

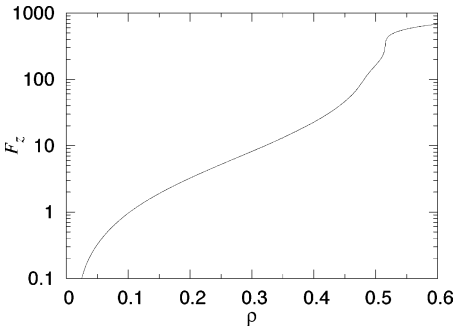

Figure 4. Relation between ρ and F_z as obtained by mapping $\rho(x = 0, z)$ against $F_z(x = 0, z)$ as given in Figure 2. Since $\rho(x, z)$ is computed on a finer grid than $F(x, z)$, this mapping involves interpolation of both functions such that the resulting mapping no longer consists of individual data points.

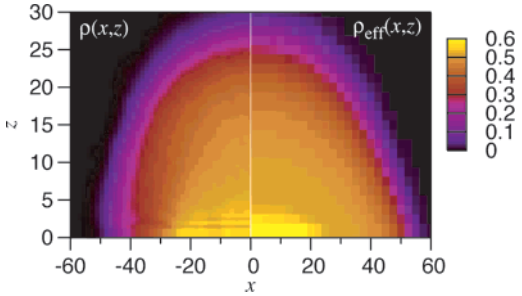

Figure 5. Density of the unperturbed brush $\rho(x, z)$ and effective brush density $\rho_{eff}(x, z)$ as obtained by a force-density mapping of the force onto the AFM tip.

density as "effective", since it is the density that would have been provided by an AFM measurement after a calibration in terms of "real" densities.

The differences between $\rho(x, z)$ and $\rho_{eff}(x, z)$ are significant. In the center, $x = 0$, the two density profiles are identical by construction. However, near the stripe edges, the difference is considerable. The brush width as deduced from the AFM measurement would significantly overestimate the real brush width. This effect is a direct reflection of the same behavior for F_z, and the same qualitative explanation as given above thus applies.

In addition to the circumference of the brush, also the width of the transition region, in which the polymer density drops from the high density in the interior of the brush to zero, is different. Figure 5 (left) shows that this transition region is twice as thick near the stripe edge as in the center of the brush for the unperturbed brush. (Remember the different x and z scales in the figures!) Considering instead $\rho_{eff}(x, z)$, this thickness would be about the same everywhere — a feature that stems from the same behavior exhibited by $F_z(x, z)$ [see Figure 2]. Near the stripe edge, $F_z(x, z)$ thus drops off faster than $\rho(x, z)$.

Also this effect is qualitatively explained by the sketch in Figure 3. When the AFM tip is pushed into the polymer brush from the side (the situation depicted in the sketch), the contact area between AFM tip and brush increases approximately linear with the displacement of the AFM tip into the brush. When the AFM tip is pushed into the brush at the center, the three-dimensional nature of the pyramid modeling the tip leads to a quadratic increase in contact area and hence an initially slower increase. The AFM tip thus needs to go a longer way near the center than near the edges before it gives the full signal. It should be stressed that this effect would be absent if the AFM tip would be incorrectly modeled as two-dimensional, neglecting the y dependence present in the combined system polymer brush−AFM tip.

C. Steric Force. The force profile $\vec{F}(x, z)$ onto the AFM tip presented so far was evaluated by explicit summation of all the pairwise interaction between polymer particles and AFM tip particles for different (x, z)-position of the tip. However, the force onto the surface of the AFM tip can also be evaluated using the pressure tensor of the *perturbed* polymer brush, $\vec{\vec{p}}(x, y, z)$, according to

$$\vec{F} = \int_{\text{surface}} \mathrm{d}^2\sigma_{\vec{r}'}\, \vec{\vec{p}}(\vec{r}')\cdot\vec{n}_{\vec{r}'} \tag{1}$$

where the integration is over the entire surface $\sigma_{\vec{r}'}$ of the tip and $\vec{n}_{\vec{r}}$ denotes the local normal vector at point $\vec{r}$.

We will now decompose the force $\vec{F}$ into two components according to

$$\vec{F} \equiv \vec{F}^{(0)} + \vec{F}^{(1)} \tag{2}$$

where $\vec{F}^{(0)}$ will be denoted as a steric component, and $\vec{F}^{(1)}$ is the remaining part. The former one is defined through eq 1 but with $\vec{\vec{p}}(x, y, z)$ replaced by the pressure tensor for the *unperturbed brush*, $\vec{\vec{p}}^{0}(x, z)$. Consequently, $\vec{F}^{(1)}$ represents the effect of the reorganization of the brush by its interaction with the AFM tip and will be denoted as the reorganization component.

To obtain $\vec{F}^{(0)}$, $\vec{\vec{p}}^{(0)}(x, z)$ was sampled from simulations of the unperturbed brush. No sampling of the pressure tensor $\vec{\vec{p}}(x, y, z)$ of the perturbed brush was made. The three-dimensional dependence would require a prohibitively long simulation. Moreover, the additional insight would be limited as eq 1 is fulfilled by definition.

The computed values of the diagonal elements of the pressure tensor $\vec{\vec{p}}^{(0)}$ of the unperturbed polymer brush are shown in Figure 6. First, without any external load, mechanical stability implies that $\langle p_{zz}^{(0)}(x, y, z)\rangle_x = 0$ for a nanopattered brush [for a homogeneously grafted polymer brush, the stronger condition $p_{zz}^{(0)}(x, y, z) = 0$ is valid], as otherwise the brush could lower its free energy by readjusting its vertical size. $p_{xx}^{(0)}$ and $p_{yy}^{(0)}$ as well as their x-averages are generally nonzero. The off-diagonal elements of $\vec{\vec{p}}^{(0)}$ were equal to zero within statistical error. This is expected as the off-diagonal components are related to shear, and a stationary shear can be sustained only within solid materials.

In the center of the brush, the polymer chains are stretched vertically as they are compressed in the $x-y$-plane by neighboring chains. Positive pressures always correspond to compression and negative pressures to elongation, and, consequently, in the center of the brush, $p_{xx}^{(0)}$ and $p_{yy}^{(0)}$ are positive whereas $p_{zz}^{(0)}$ becomes negative. Near the edges, the compression appears in the y- and z-directions with $p_{yy}^{(0)}$ and $p_{zz}^{(0)}$ being positive, and the stretching is predominantly along the x-direction, where a negative $p_{xx}^{(0)}$ is observed. Hence, the profiles of the diagonal components of the pressure tensor are clearly related to the compression/stretching of the chains. When considering the orientational averaged pressure $p_{iso}^{(0)}$, much of this detail is lost, and the pressure profile resembles the density profile.

An evaluation of the force $\vec{F}^{(0)}$ from the pressure tensor is incomplete as long as the rigid structure of the AFM tip is not explicitly taken into account. The force onto the surfaces can induce an internal stress that in turn is able to redirect the pressure along the x-direction into a force in the z-direction, acting toward the mounting point of the tip.

The total force onto the AFM tip is most easily calculated by determining the work needed to move the tip in the

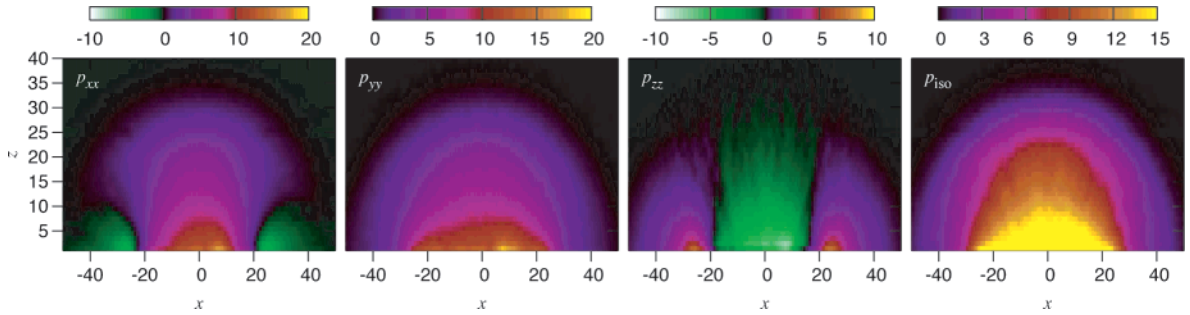

Figure 6. Diagonal elements of the pressure tensor $\vec{p}^{(0)}(x, z)$ and their isotropic average $p_{iso}^{(0)}(x, z) = \mathrm{tr}\,[\vec{p}^{(0)}(x, z)]/3$ of an unperturbed brush.

z-direction. First, we need the force F_x^r acting onto the right facet of the AFM tip, given by

$$F_x^r = \int_{\text{facet}} d\sigma_{\vec{r}}\, p_{xx}^{(0)}(\vec{r}\,')\cos\alpha \tag{3}$$

The integration over $\sigma_{\vec{r}'}$ can be replaced by an explicit integration over y' and z'. For an AFM tip positioned at (x, y, z), $x' = x + (z' - z)\tan\alpha$, hence

$$F_x^r = \int_z^\infty dz' \int_{y-(z'-z)\tan\alpha}^{y+(z'-z)\tan\alpha} dy'\, p_x^{(0)}(x + [z' - z]\tan\alpha, y', z') \tag{4}$$

A factor of $1/\cos\alpha$ appears in the conversion from $\sigma_{\vec{r}'}$ to y' and z' going from eq 3 to eq 4.

If the AFM tip is moved downward by a distance Δz, the right facet of the tip will move to the right by a distance Δx

$$\Delta x = \Delta z \tan\alpha \tag{5}$$

In the process, the AFM tip has to perform work $\Delta W^r = F_x^r \Delta x$ against the polymer brush. This work has to be identical to work performed by pressing down the AFM tip, $\Delta W^r = F_z^r \Delta z$, and hence

$$F_z^{r\prime(0)} = \tan\alpha F_x^r \tag{6}$$

In addition, there is also a direct effect from p_{zz}

$$F_z^r = \int_z^\infty dz' \int_{y-(z'-z)\tan\alpha}^{y+(z'-z)\tan\alpha} dy'\, p_{zz}^{(0)}(x + (z' - z)\tan\alpha, y', z') \tag{7}$$

Hence, the expression for the force has the same form as for F_x^r as the different geometric prefactors cancel. Adding this contribution to eq 6 yields

$$F_z^{r\prime(0)} = F_z^r + \tan\alpha F_x^r \tag{8}$$

Similar results follow for the other three facets. In the equations so far, explicit integrations over y' have been left in place to ensure symmetry among the expressions for all four facets. As the unperturbed brush possesses no y dependences, the integrals over y' appearing in the expressions for the right and the left facet can be eliminated. Collecting results, one arrives at

$$\begin{aligned} F_z^{(0)} = 2\tan\alpha \int_z^\infty dz'\,(z' - z)[&\tan\alpha\, p_{xx}^{(0)}(x + [z' - z]\tan\alpha, z') + \tan\alpha\, p_{xx}^{(0)}(x - [z' - z]\tan\alpha, z') + \\ &p_{zz}^{(0)}(x + [z' - z]\tan\alpha, z') + p_{zz}^{(0)}(x - [z' - z]\tan\alpha, z')] + \\ 2\int_z^\infty dz' \int_{x-(z'-z)\tan\alpha}^{x+(z'-z)\tan\alpha} dx'\,&[\tan\alpha\, p_{yy}^{(0)}(x', z') + p_{zz}^{(0)}(x', z')] \end{aligned} \tag{9}$$

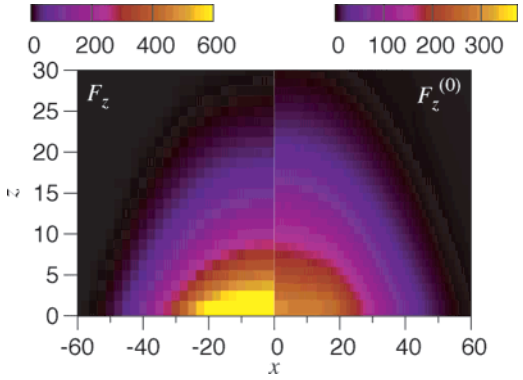

Figure 7. Vertical force F_z and its steric component $F_z^{(0)}$ as evaluated from eq 9 and the pressure tensor for an unperturbed brush. Note, different color coding is used, implying that $F_z^{(0)}$ is about half as large as F_z.

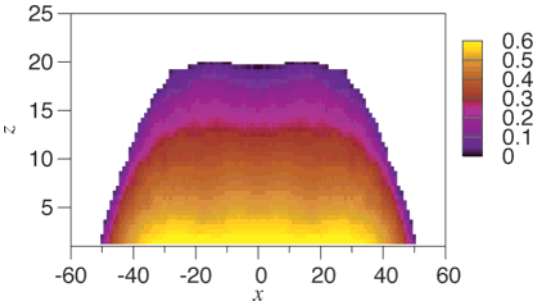

Figure 8. Ratio $F_z^{(1)}/F_z$ of the total vertical force that is due to reorganization inside the polymer brush.

Evaluation of eq 9 using the pressure tensor $\vec{p}^{(0)}$ given in Figure 6 gives the steric force estimate $F_z^{(0)}$ shown in Figure 7 (right). As all nonbonded forces are purely repulsive, the brush cannot pull down the AFM tip, and consequently the parts of the integration with $p_{zz}^{(0)} < 0$ were ignored.

A comparison of F_z and $F_z^{(0)}$ shows that about half of the vertical force originates from the pressure of the unperturbed brush. This implies that the remaining part $F_z^{(1)}$, originating from the reorganization of the brush, is of equal magnitude. In more detail, we find (cf. Figure 8) that $F_z^{(0)}$ is only about one-third of F_z in the high force region close to the surface whereas $F_z^{(0)} \approx F_z$ at the interface of the brush. Consequently, the reorganization contribution $F_z^{(1)} \equiv F_z - F_z^{(0)}$ is largest close to the grafting surface where the end-grafting prevents a long-distances spatial reorganization of the polymers while the polymers have much more freedom near the brush interface. The dependence on x is only minor, thereby confirming that it is the grafting and not the excluded-volume interaction that limits the ability of the brush to reorganize.

The independence on x implies that the importance of the reorganization effect for the total force onto the AFM tip

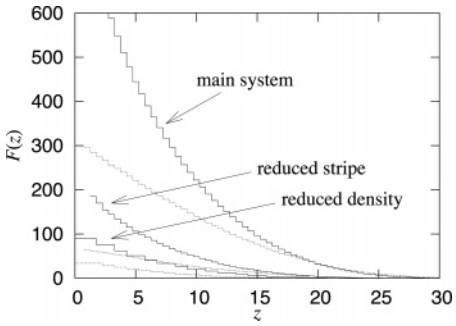

Figure 9. Total force $F(z)$ (solid lines) and its steric component $F^{(0)}(z)$ (dashed lines) in the center of the polymer brush for the main system studied in this paper, a brush where the stripe width Δ is reduced by 60%, and a brush where the grafting density σ is reduced by 60%.

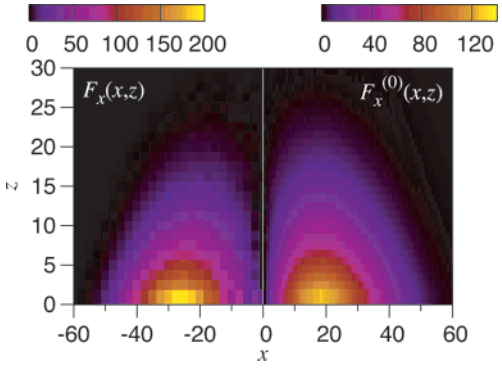

Figure 10. Horizontal force F_x and its steric component $F_x^{(0)}$ as evaluated using eq 10 and the pressure tensor for an unperturbed brush. Note, different color coding is used, implying that $F_x^{(0)}$ is about half as large as F_x.

depends only moderately on Δ or σ as these two parameters determine the width of the transition region near the edge of the pattern.[12] We have confirmed this by two additional studies: in the first, the width of the stripe is reduced by 60%; in the second, the grafting density is reduced by 60% keeping $\Delta = 50$. In Figure 9, we compare the total force $F(z)$ and its its steric component $F^{(0)}(z)$ in the center of the brush ($x = 0$), for all three systems. As expected, the absolute values of the forces differ strongly between the three systems. The ratio between $F(z)$ and $F^{(0)}(z)$ near the grafting surface, however, is the almost the same for all three systems: $35 \pm 5\%$ of the total force comes from the steric component, and the remainder comes from the brush reorganization.

D. Horizontal Force. Apart from the repulsive vertical force F_z acting on the AFM tip, a horizontal force also acts onto the tip. By symmetry, $F_y = 0$ throughout the entire brush, whereas $F_x(z)$ is generally nonzero. Figure 10 (left) shows the F_x from the explicit simulations. By symmetry $F_x(x = 0, z) = 0$ and at the edges of the brush F_x becomes zero again due to the lack of polymer matter. Hence, in the region in between, F_x displays a maximum.

A comparison of F_x in Figure 10 (left) and F_z Figure 7 (left) shows that both force components are of comparable magnitude. We found that the ratio $F_x(x, z)/F_z(x, z)$ is almost independent of z and increases approximatively as x^2, and in the outer 20% of the brush, F_x is larger than F_z. The details of the AFM apparatus will affect if and/or how the horizontal force influences the measurement process.

Using the same sequence of arguments as in section III.C, the steric component of F_x can be computed from the unperturbed pressure tensor $\vec{p}^{(0)}$. Because of the opposite orientation of the normal vector on opposite facets of the AFM tip, effectively the relevant quantity is the gradient $\partial p_{xx}^{(0)}(x, z)/\partial x$. Numerically, the force can be expressed as

$$F_x^{(0)} = 2 \tan\alpha \int_z^\infty dz' (z' - z)[p_{xx}^{(0)}(x + [z' - z]\tan\alpha, z') - p_{xx}^{(0)}(x - [z' - z]\tan\alpha, z')] \quad (10)$$

and the result is shown in Figure 10 (right). Basically, $F_x^{(0)}$ is half of F_x. Hence, the divisions into steric and reorganization components are similar for the vertical and horizontal forces.

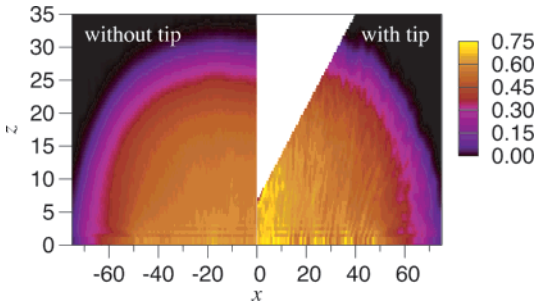

Figure 11. Density profile of an unperturbed brush $\rho(x, z)$ and of a perturbed brush $\rho_{pert}(x, z)$, where the space occupied by the AFM tip is indicated by the white area. In the former case, average was made over the full y-axis, whereas in the latter case, a narrow slice including the apex of the AFM tip was used implying larger statistical uncertainty due to the much smaller volume involved.

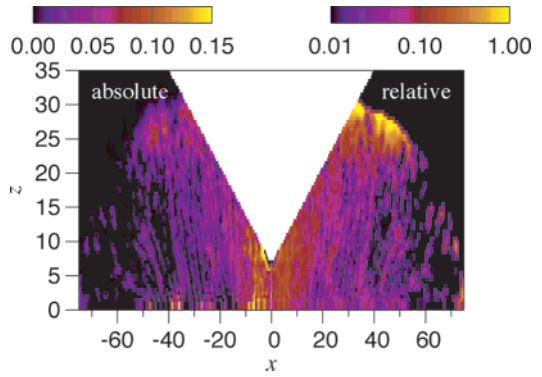

Figure 12. Absolute difference $\rho_{pert}(x, z) - \rho(x, z)$ and relative difference $[\rho_{pert}(x, z) - \rho(x, z)]/\rho(x, z)$ between the density profiles of the perturbed and unperturbed brushes.

E. Brush Reorganization. We will now briefly discuss how the brush is reorganized by the presence of the AFM tip. For this, we consider a patterned brush with width $\Delta = 100$, i.e., twice as wide as for the simulations presented so far. This ensures that a plateau has formed in the center of the brush[12] and thus allows one to better distinguish between compression and displacement of polymer matter.

Figure 11 shows the density profiles the brush polymer brush in the absence (left) and in the presence (right) of the AFM tip. The latter profile is averaged over a slice passing through the apex of the AFM tip, making the statistical uncertainty larger. The effects of the reorganization are smaller if slices not running through the AFM tip apex would be considered.

The differences between the density profiles for the perturbed and unperturbed brushes are best illustrated using the absolute and relative density differences as presented in Figure 12. The change of the polymer brush induced by contact with the AFM tip is 3-fold. There is a moderate increase of the density throughout a significant part of the brush which does not depend that much on position. Second, the brush interface is moved somewhat outward, in particular far from the surface (large z). These two effects are coupled and can be interpreted as a linear

response — the reduction of the available volume by the AFM tip is compensated for by the polymer matter moving outward with a small increase in density as the driving force. The overall structure of the brush as such is not changed much by these processes, however. Finally, near the apex of the AFM tip a larger increase in the density appears. Here, as explained above, the grafting restricts the polymer's ability to be displaced away from the AFM tip to a larger degree. This can be understood as a position-dependent compressibility modulus. In other words: near the grafting surface, the brush is much harder than near the interface.

IV. Conclusions

In contrast to a conventional, homogeneously grafted polymer brush, a nanopatterned polymer brush possesses a richness of internal structure. In different regions of the patterned brush, polymer segments are stretched and/or compressed in different directions. This is reflected well in the pressure tensor profiles that we have computed. This structure is completely absent in the density profile, however. While the properties of a homogeneously grafted polymer brush can be understood from its density profile alone, this thus no longer is possible for a nanopatterned brush, and more information, such as the pressure tensor profile, is needed.

The interaction between an AFM tip and a polymer brush is heavily influenced by steric effects from the shape of the AFM tip. While this in itself is obvious and applies to any kind of AFM measurement, the qualitative and quantitative consequences for nanopatterned systems had been unknown. Using the pressure tensor profiles, the steric force computed from a folding of the AFM tip geometry and brush properties gives a quantitative agreement in the outer regions of the brush where more than 90% of the force onto the AFM tip can be explained from it. This also proves the applicability of the concepts and assumptions of this approach.

Upon contact between the AFM tip and the polymer brush, the brush will deform. While this in itself is interesting from a fundamental point of view as it gives valuable information about the properties of the brush, it is often problematic in experiments as the aim usually is to study the unperturbed brush. While we cannot compute (the change of) the force $F^{(1)}$ onto the AFM tip due to this reorganization directly, our ability to compute the force $F^{(0)}$ due to the unperturbed brush by means of the pressure tensor profile still allows us to quantify this effect. For this approach to work, it is necessary that we are able to compute $F^{(0)}$ to very good approximation. This is the case as seen by the agreement between $F^{(0)}$ and the directly calculated force F in the outer regions of the brush. The use of a simpler theory (e.g., based on the density profile only instead of the pressure tensor) to compute $F^{(0)}$ would not be sufficient.

While we find that the reorganization effect is dominant far in the inside of the nanopatterned brush, it becomes minor near the brush interface. Since it is the latter that is usually probed in experiments, inclusion of reorganization effects is not needed for understanding of the results. Inclusion of the steric effect of the AFM tip geometry is, in contrast, essential. The virtual shape of the patterned polymer brush (as measured by AFM) is changed as its sides become straight lines with the same slope as the slope of the AFM tip. This makes the virtual polymer brush wider than the real polymer brush. For typical parameter values, this overestimation of the brush width is of order 25% of the polymer contour length. It should be noted that, somewhat counterintuitively, these effects become stronger as the grafting density σ is decreased.

Acknowledgment. We thank Stefan Zauscher for valuable discussions and acknowledge financial support from the European Union (Contract No. MRTN-CT-2004-512331) and the Swedish Foundation for Strategic Research (SSF).

Appendix A: Model and Methods

All nonbonded interactions between particles, independent of whether they belong to the polymer or to the AFM tip, are modeled by the purely repulsive Lennard-Jones potential

$$V_{\mathrm{LJ}}(r) = \begin{cases} 4\epsilon\left[\left(\frac{\tilde{\sigma}}{r}\right)^{12} - \left(\frac{\tilde{\sigma}}{r}\right)^{6} + \frac{1}{4}\right] & \text{if } r \le 2^{1/6}\tilde{\sigma} \\ 0 & \text{if } r \ge 2^{1/6}\tilde{\sigma} \end{cases} \quad \text{(A1)}$$

where r is the particle separation and $\tilde{\sigma}$ and ϵ are the two Lennard-Jones parameters. Bonded interactions are modeled by a stiff harmonic potential

$$V_{\mathrm{bond}}(r) = 1000\frac{\epsilon}{\tilde{\sigma}^2}(r - \tilde{\sigma})^2 \quad \text{(A2)}$$

A repulsive potential is used to prevent the particles from entering the planar surface at $z = 0$. The temperature is set to $k_{\mathrm{B}}T/\epsilon = 1$. Throughout, we use $\tilde{\sigma}$ as the length scale and ϵ as the energy scale. All derived units follow from this choice of units. Notably, for ambient temperature and realistic choices of $\tilde{\sigma}$ and ϵ, a unit force corresponds to about 1 pN. Our results compare well to AFM experiments where a contact between the AFM tip and the brush is usually detected at a force of order 50 pN.

At first, a single simulation of the polymer brush without the presence of an AFM tip is run for equilibration. Polymers are grafted at random positions on an area of size $N \times N$, where all grafting points have a mutual distance of at least 1. Periodic boundary conditions in y-direction are applied.

Using this equilibrated structure, the AFM tip is first placed at some x-coordinate above the brush. The tip is then lowered by 0.25 length units toward the brush, followed by energy minimization to remove close contacts, and the procedure is repeated until the tip is touching the grafting surface. This gives initial structures for the subsequent simulations, with the AFM tip at the desired position. These simulations lasted for 1000 time units (one million integration steps). The AFM tip was kept stationary, and the force onto the tip was computed from explicit summation of all forces between particles in the brush and the tip. As the energy minimization process leaves a structure far away from equilibrium, half of the simulation time is set aside for equilibration, and only the second half is used for data analysis. The force onto the AFM tip was computed as a function of tip position (x, z) using a 25 by 28 grid for the tip position, where symmetry was already employed to remove tip positions with $x < 0$. This large number of independent simulations makes this a significant numerical task that is much more expensive than earlier simulations on homogeneously grafted polymer brushes.

The simulations were performed using the Gromacs molecular dynamics suite.[23] The pressure tensor $\vec{p}^{(0)}(x, z)$ was computed using a version of the Gromacs code[24] that we extended to compute simultaneously the x and z dependence and the off-diagonal elements. A canonical ensemble was sampled by use of a Berendsen thermostat.[25]

In addition to the simulations of the interaction between the polymer brush and the AFM tip, simulations of the polymer

brush without the AFM tip were performed to determine density and two-dimensional pressure tensor profiles of the unperturbed brush.

References and Notes

(1) Dyer, D. J. *Adv. Funct. Mater.* **2003**, *13*, 667−670.
(2) Gates, B. D.; Xu, Q.; Stewart, M.; Ryan, D.; Willson, C. G.; Whitesides, G. M. *Chem. Rev.* **2005**, *105*, 1171−1196.
(3) Kawaguchi, M.; Takahashi, A. *Adv. Colloid Inter. Sci.* **1992**, *37*, 219−317.
(4) Binnig, G.; Quate, C. F. *Phys. Rev. Lett.* **1986**, *56*, 930−933.
(5) Magonov, S. N.; Reneker, D. H. *Annu. Rev. Mater. Sci.* **1997**, *27*, 175−222.
(6) García, R.; Pérez, R. *Surf. Sci. Rep.* **2002**, *47*, 197−301.
(7) Kaholek, M.; Lee, W.-K.; LaMattina, B.; Caster, K. C.; Zauscher, S. In *Polymer Brushes*; Advincula, R. C., Brittain, W. J., Caster, K. C., Rühe, J., Eds.; Wiley-VCH: Weinheim, Germany, 2004; pp 381−402.
(8) Wilder, K.; Quate, C. F.; Singh, B.; Alvis, R.; Arnold, W. H. *J. Vac. Sci. Technol. B* **1996**, *14*, 4004−4008.
(9) Cappella, B.; Dietler, G. *Surf. Sci. Rep.* **1999**, *34*, 1−104.
(10) Kelley, T. W.; Schorr, P. A.; Johnson, K. D.; Tirrell, M.; Frisbie, C. D. *Macromolecules* **1998**, *31*, 4297−4300.
(11) Butt, H.-J.; Cappella, B.; Kappla, M. *Surf. Sci. Rep.* **2005**, *59*, 1−152.
(12) Patra, M.; Linse, P. *Nano Lett.* **2006**, *6*, 133−137.
(13) Aimé, J. P.; Elkaakour, Z.; Odin, C.; Bouhacina, T.; Michel, D.; Curély, J.; Dautant, A. *J. Appl. Phys.* **1994**, *76*, 754−762.
(14) Murat, M.; Grest, G. S. *Macromolecules* **1996**, *29*, 8282−8284.
(15) Hirai, Y.; Konishi, T.; Yoshikawa, T.; Yoshida, S. *J. Vac. Sci. Technol. B* **2004**, *22*, 3288−3293.
(16) Yoshimoto, K.; Jain, T. S.; Workum, K. V.; Nealey, P. F.; de Pablo, J. J. *Phys. Rev. Lett.* **2004**, *93*, 175501.
(17) Jeon, S. I.; Lee, J. H.; Andrade, J. D.; Gennes, P. G. D. *J. Colloid Interface Sci.* **1991**, *142*, 149−158.
(18) Jeon, S. I.; Andrade, J. D. *J. Colloid Interface Sci.* **1991**, *142*, 159−166.
(19) Subramanian, G.; Williams, D. R. M.; Pincus, P. A. *Macromolecules* **1996**, *29*, 4045−4050.
(20) McCoy, J. D.; Curro, J. G. *J. Chem. Phys.* **2005**, *122*, 164905.
(21) Steels, B. M.; Koska, J.; Haynes, C. A. *J. Chromatogr. B* **2000**, *743*, 41−56.
(22) Pang, P.; Koska, J.; Coad, B. R.; Brooks, D. E.; Haynes, C. A. *Biotechnol. Bioeng.* **2005**, *90*, 1−13.
(23) Lindahl, E.; Hess, B.; van der Spoel, D. *J. Molecular Modeling* **2001**, *7*, 306−317.
(24) Lindahl, E.; Edholm, O. *J. Chem. Phys.* **2000**, *113*, 3882−3893.
(25) Berendsen, H. J. C.; Postma, J. P. M.; van Gunsteren, W. F.; Di Nola, A.; Haak, J. R. *J. Chem. Phys.* **1984**, *81*, 3684−3690.

MA0606410